Published in final edited form as:
Bioconjug Chem. 2008 June ; 19(6): 1211–1218. doi:10.1021/bc800015n.

NanoFerrite Particle Based Radioimmunonanoparticles: Binding affinity and in vivo pharmacokinetics

A. Natarajan[†], **C. Gruettner**[‡], **R. Ivkov**[§], **G. L. DeNardo**[†], **G. Mirick**[†], **A. Yuan**[†], **A. Foreman**[§], and **S. J. DeNardo**[†]

[†]School of Medicine, University of California Davis, Sacramento, California, USA

[‡]Micromod Partikeltechnologie, GmbH, Rostock-Warnemuende, Germany

[§]Triton BioSystems, Inc., Chelmsford, Massachusetts, USA

Abstract

Dextran and PEG coated iron oxide nanoparticles (NP), when suitably modified to enable conjugation with molecular targeting agents, provide opportunities to target cancer cells. Monoclonal Antibodies, scFv, and peptides conjugated to 20-nm NP have been reported to target cancer for imaging and alternating magnetic field (AMF) therapy. The physical characteristics of NP's can affect their in vivo performance. Surface morphology, surface charge density, and particle size are considered important factors that determine pharmacokinetics, toxicity, and biodistribution. New NanoFerrite (NF) particles having improved specific AMF absorption rates and diameters of 30 nm and 100 nm were studied to evaluate the variation in their in vitro and in vivo characteristics in comparison to the previously studied 20 nm Superparamagnetic Iron Oxide (SPIO) NP. SPIO NP 20-nm, NF NP 30- and 100-nm were conjugated to ^{111}In-DOTA-ChL6, a radioimmunoconjugate. Radioimmunoconjugates were conjugated to NP's using 25μg of RIC/mg of NP by carbodiimide chemistry. The radioimmunonanoparticles (RINP) were purified characterized by PAGE, cellulose acetate electrophoresis (CAE), live cell binding assays, and pharmacokinetics in athymic mice bearing human breast cancer (HBT 3477) xenografts. RINP (2.2 mg) were injected iv and whole body, blood and tissue data were collected at 4, 24, and 48 hours. The preparations used for animal study were >90% monomeric by PAGE and CAE. The immunoreactivity of the RINP was 40−60% compared to ^{111}In-ChL6. Specific activities of the doses were 20−25μCi/2.2 mg and 6−11μg of MAb/2.2 mg of NP. Mean tumor uptakes (% ID/g ± SD) of each SPIO 20nm, NF 30nm, and 100nm RINP at 48h were 9.00 ± 0.8 (20nm), 3.0 ± 0.3 (30nm), and 4.5 ± 0.8 (100nm) respectively; the ranges of tissue uptakes were liver (16−32 ± 1 − 8), kidney (7.0−15 ± 1) spleen (8−17 ± 3 − 8) lymph nodes 5 − 6 ± 1 −2) and lung (2.0− 4 ± 0.1 − 2). In conclusion, this study demonstrated that 100 nm NF NP could be conjugated to ^{111}In-MAb so that the resulting RINP had characteristics suitable for AMF therapy. Although 100-nm RINP targeted tumor less than 20-nm SPIO RINP, their heating capacity is typically 6 times greater, suggesting the 100-nm NF RINP could still deliver better therapy with AMF.

Keywords

Nanoparticle; NanoFerrite particles; ^{111}In-ChL6, immunoreactivity; radioimmunonanoparticles

Corresponding Author: Arutselvan Natarajan PhD Radiodiagnosis & Therapy Molecular Cancer Institute 1508 Alhambra Blvd., Room 3100 Sacramento, CA 95816 Phone: 916−734−3787 Fax: 916−703−5014 E-mail: arutselvan.natarajan@ucdmc.ucdavis.edu.

INTRODUCTION

Dextran and PEG coated magnetic iron oxide nanoparticles linked to a fluorescent or radiolabeled molecular targeting agent have been used to a) deliver heat selectively at the microenvironment of tumors with external AMF b) construct the multiple mono or bi-specific targeting units and c) image and trace the NP kinetics in vivo (1-5). Systemic delivery of nanoparticles specifically to cancer tissues in concentrations sufficient to achieve therapeutic thermal dose induced by external alternating magnetic field has also been demonstrated to be predicted by calculated heat dosimetry (5;6). This can allow specific heating of cancer tissues using RINP by AMF providing a promising treatment modality (7). Radioactivity quantitation should provided sufficient concentration of the particles is retained in the tumor tissue relative to nearby normal tissues, and the particles characteristics specific AMF absorption rate (SAR), to allow calculations of selective heat generation in tumor with moderate AMF amplitudes.

Exposure of tissue to alternating magnetic fields results in the deposition of heat through the induction of eddy currents in tissues that is dependent upon the field frequency, amplitude, duration of exposure, and area of exposed tissue (5). This induced heating can be controlled and minimized through judicious selection of AMF parameters, and when combined with appropriately targeted particles can lead to successful therapy. Thus, successful therapy requires an appropriate combination of AMF parameters be directed to tumor tissue that contains a sufficiently high concentration of particles capable of producing therapeutic heat at the chosen AMF amplitudes, and minimizing both AMF exposure and particle concentrations in nearby surrounding tissues. In this manner, cytotoxic heat can be deposited specifically into the tumor microenvironment while simultaneously minimizing the non-specific heating of surrounding healthy tissues.

The elevation of tissue temperature to between 40 °C and 45 °C is often called hyperthermia (8). There is a clear rationale for using hyperthermia in cancer treatment because hyperthermia is known to cause direct cytotoxicity and because it also acts as a radiation and chemo sensitizer (8). However, there is generally no intrinsic difference between hyperthermia sensitivity of normal and tumor cells, except for hematological malignancies (9). On the other hand, selective tumor cell kill can be achieved *in vivo* in this range because of characteristic differences between normal and tumor physiology. The architecture and vasculature in solid tumors is chaotic producing hypoxic and low pH [2 − 4] conditions that sensitize cells to thermal damage.

The effect of hyperthermia depends upon the achieved temperature and time of exposure. At temperatures above 42.5 − 43 °C, the exposure time can be halved with each 1 °C temperature increase to give an equivalent cell kill (9;10). Hyperthermia inhibits cellular repair of sub lethal radiation damage and also induces increasing radiosensitivity due to tumor reoxygenation. Despite the beneficial attributes of hyperthermia for cancer treatment, its clinical application has been limited because of a general inability to a) deliver sufficient heat selectively to the tumor tissue, and b) accurately predict or measure heat dose deposited in the tumor (8-10).

Tumor targeted heat therapy using the combination of NP and AMF has the potential to overcome both these limitations. In a previous study, 20-nm dextran matrix nanoparticles containing super paramagnetic iron oxide were linked to breast cancer targeting chimeric L6 (ChL6) monoclonal antibody (bioprobe) demonstrated the feasibility of delivering thermo ablation to cancer cells (5). More key to clinical application of NP/AMF therapy was the demonstration of heat thermal dosimetry was predictive of tumor response and minimal normal tissues toxicity (7).

In order to further raise the therapeutic index of tumor response without normal tissue toxicity an increased heat dose is needed. The heat dose (Joules/g of tumor tissue) can be increased by a combination of increased particle concentration in the tumor and/or increasing the heat output of the particles. The latter can be achieved only with higher SAR particles because increasing heat from the particles by using higher AMF amplitudes duration of exposure, increases the potential for non-specific heating (5;7;11).

New NF particles with high specific AMF absorption rates were synthesized by high-pressure homogenization according to a core-shell method, having a range of sizes (20 to 100 nm) (12). Selected NF particles 30 and 100nm were synthesized and characterized for the present study; measured specific absorption rates (SAR) demonstrated 7−10 times higher SAR at various AMF amplitudes and 150 kHz than 20 nm SPIO particles (12). The NF particles possess an iron oxide core (density >5 g/cm^3), (10 − 60 nm) that is surrounded by a dextran shell. The iron content of the particles is >50% w/w, and they are separable with a permanent magnet. The dextran shell was further modified by cross linking and addition of carboxyl terminated PEG (PEG-COOH) for antibody conjugation (12).

By contrast, the previously described 20-nm SPIO particles are produced by the precipitation of ferric and ferrous chlorides in the presence of dextran (13-15). These particles consist of <40% w/w iron in a dextran matrix that is not cross linked. Separation can be achieved only with the use of a high gradient magnetic field, thus they are not separable with a permanent magnet. SAR values produced by these particles have been measured to range from 27 − 105 Watts per gram iron (12), several times lower than that observed with the NF particles.

Because of the significantly different physical and magnetic characteristics exhibited by the NF and SPIO particles, the potential utility of NF-based RINP's for cancer therapy must be validated with a study of their *in vivo* performance after conjugation with a monoclonal antibody (ChL6). This report describes the development of ^{111}In-ChL6 linked to various NP's: 20-nm SPIO, 30-nm NF, and 100-nm NF to produce RINP. Mean RINP diameter and size distributions were measured by photon correlation spectroscopy. *In vitro* and *in vivo* targeting and pharmacokinetics (PK) of the RINP's were characterized. The in vivo tumor targeting and in vitro SAR data were compared for the various RINP's to predict thermal dose deliverable at the cancer tissues by various AMF amplitudes (at 150 kHz) to enhance further development of optimal particles for future NP-AMF thermal therapy.

EXPERIMENTAL PROCEDURES

Materials

Carrier-free ^{111}In (MDS Nordion, Ontario, Canada) was purchased as $^{111}InCl_3$ in 0.05 M HCl. Chimeric L6 (ChL6), human-mouse monoclonal antibody chimera (Bristol-Myers Squibb Pharmaceutical Research Institute, Seattle, WA), reacts with an integral membrane glycoprotein highly expressed on human breast, colon, ovary, and lung carcinomas (16;17). ChL6 was specified as greater than 95% pure monomeric IgG by polyacrylamide gel electrophoresis (PAGE). High gradient magnetic field (HGMF) columns and separator, Nanomag®-D-SPIO 20nm (product #: 79−56−201) and COOH functionalized, dextran and polyethylene glycol (PEG) coated NF particles of 30 nm (84−56−301), and 100nm (84−56−102) particles in suspension (15−25 mg/ml) were obtained from micromod Partikeltechnologie, GmbH (Rostock, Germany). MES (2-(4-morpholino) ethanesulphonic acid), EDC (1-ethyl-3- (3-dimethylaminopropyl)-carbodiimide HCl), NHS (N-hydroxysuccinimide), glycine, and PBS were purchased from Sigma Chemical Co., (St. Louis, MO). EDC activated NPs were purified by membrane dialyzer 3400 kDa cut off (Pierce, Rockford, IL) dialysis bags. *S*-2-(4-isothiocyanatobenzyl) −1, 4, 7, 10-

tetraazacyclododecane-N, N', N'', N''-tetraacetic acid (DOTA-Bz-SCN) was purchased from Macrocyclics. (Dallas, TX).

Preparation of SPIO and NanoFerrite particles (NF)

SPIO particles were prepared by the precipitation of ferric and ferrous chlorides in the presence of dextran (13-14). NF particles (International and European patent #s WO 2005006356, WO 20050271745 and DE 10331439) were synthesized by high-pressure homogenization by core–shell method (12). Briefly, a monodisperse aqueous iron oxide suspension (25 mg/ml) was homogenized with an excess of dextran at pressures above 500 bar and at temperatures above 70° C, for 30 min. NF particles with iron content 45% (w/w) were obtained after magnetic sedimentation in a crystallization disk at NdFeB permanent magnet and washing with deionized water. The NF particles were cross linked by a modified Josephson method (18) with a mixture of poly (ethylene glycol) diglycidyl ether, and epichlorohydrin at pH 11−12 for 24 h at room temperature. After magnetic separation particles were washed with deionized water, and NF particle suspension with an iron concentration of 20−25 mg/ml was obtained. The particles were functionalized with amino groups by shaking with ammonia at room temperature for 24 h. The amine functionalized NF particles were further washed three times with deionized water by magnetic separation and filtered through 0.22 mm Millex-GP filters (Millipore). These NF particles were further modified by EDC and polyethylene glycol 600 diacid using MES buffer (pH 6.3) and incubated for 2 h at room temperature for COOH functionalization. The narrow size distributions of the NF particles obtained were in two diameter ranges of 20−40 and 80−100 nm (12).

Preparation of Radioimmunoconjugate (RIC)

The immunoconjugate (DOTA-Bz-ChL6) was prepared by previously described method (19), with slight modifications. Conjugation was carried out with final concentrations of 0.15mM ChL6 (20mg/ml) and 2.0 mM DOTA-Bz-SCN mixed in 0.1 M tetramethylammonium phosphate, pH 9, at 37 °C with 2 h incubation. The DOTA-Bz-ChL6 conjugate was purified by G50 molecular sieving chromatography and transferred to 0.1 M ammonium acetate, pH 5.3. The RIC preparation was carried out using ^{111}In chloride in 0.05 M HCl (0.2GBq) buffered in 0.1 M ammonium acetate at pH 5.3, and DOTA-Bz-ChL6 (2.5mg) added. The solution was incubated for 30 min at 37 °C, and then 0.1 M sodium ethylene diaminetetraacetate (EDTA) (Fisher Scientific, Pittsburgh, PA) was added to a final concentration of 10 mM to scavenge nonspecifically bound ^{111}In. ^{111}In-DOTA-Bz-ChL6 was purified from ^{111}In-EDTA by molecular sieving chromatography.

The reaction mixture of RIC was purified by molecular sieving (Penefsky) column. Purity was estimated by HPLC (Beckman Coulter System Gold 128, Fullerton, CA) with radioactive detector (Raytest USA, Wilmington, NC) using SEC 3000 column (GE Health care) eluted at 1 ml per minute by phosphate buffer solution. The yield and quality assurance (QA) of the RIC were evaluated by HPLC, and cellulose acetate electrophoresis (CAE) strips (Gelman Sciences Inc, Ann Arbour, MI) performed on 0.05M sodium barbital buffer at pH 8.6. The RIC bands on CAE strips and TLC plates were exposed on phosphor imager plates and scanned by Fuji Film imager (BAS 1800 II). The data was converted as digital peaks by Fuji film MultiGaugeV2.1 software.

Preparation of RINP

Three lots of nanoparticles 20-nm SPIO and 30- and 100- nm NF (12) were used for the conjugation of RIC to study in vitro targeting effect and in vivo mouse studies. ^{111}In-DOTA-Bz-ChL6 was conjugated with the nanoparticles via amide linkage to the carboxyl (COOH) terminated coating to prepare the ^{111}In-ChL6 NP. For each of the preparations, 6

mg of EDC and 12 mg of NHS in 0.5 ml of 0.5M MES buffer were mixed with 5ml of 10mg/ml of NP. This suspension was incubated for 1 h at RT with continuous mixing, then placed into 3400 MWCO dialysis bags, and dialyzed against 4 liters of saline for 1 h. ^{111}In-DOTA-Bz-ChL6 (0.5 mCi/0.2 mg/0.2 ml of PBS) suspended in 0.3 ml of 0.1 M MES buffer, was mixed with the activated SPIO and NF particles suspension and incubated for 1 h at RT with continuous mixing (20−25μg ^{111}In-ChL6/mg of NP). The preparations of 20-nm SPIO and 30-nm NF particles conjugated ^{111}In-DOTA-Bz-ChL6-NP, 2 ml, were again placed into a dialysis bags (3400 MWCO) (3 ml), and dialyzed against 4 liter of saline at RT for 1h. The 100-nm BNF particles nm was purified by magnetic separation. The RINP products were mixed with 20 ml of 25 mM glycine in PBS at RT (15 min), and then purified by high grade magnetic field (HGMF) column (20 and 30 nm) and magnetic separator (100 nm) using PBS to remove the non-bound ^{111}In-DOTA-Bz-ChL6. Non immunoreactive RINP (negative control) was prepared by similar method except the RIC used for conjugation to NP was non immunoreactive.

The final suspensions that were collected from the magnetic column or separator with PBS wash after removing from the magnetic field were brown and yielded 3−5 μg of ^{111}In-ChL6/ mg with specific activities of 6−10 μCi/mg of RINP. The concentration of the particles was estimated by UV/VIS spectrophotometry at a wavelength of 492 nm using unconjugated beads as a reference, and protein concentration was estimated at a wavelength of 280 nm and also calculated from decay corrected radioactivity. Two μl of final products were applied to multiple CAE strips for electrophoresis of 11 and 45 minutes.

Preparation of nontargeted radionanoparticles (RNP)

The nontargeted RNP (negative control) was prepared by conjugation of radiolabeled ^{111}In-DOTA-Bz-NH_2 to COOH functionalized 20 nm NP via amide linkage according to published procedure (20). Briefly, the ^{111}In-DOTA-Bz-NH_2(1.5×10^{16} molecules; 5 mCi/20 μg) diluted in 0.5 mL of 0.1 mM MES buffer was mixed to carbodiimide activated NP suspension, and incubated for 2 hours at room temperature with continuous mixing (reaction ratio was 6×10^{14} molecules of DOTA/mg of NP). The radiolabeled ^{111}In-DOTA-Bz-NP, was purified by 3,400 MW cut off dialysis membrane against 4 L of saline at RT for 1 hour. After one hour the dialyzed product was quenched with glycine (25mM) for 15 minutes to terminate remaining active sites on the particle surface. This suspension was further purified by high-gradient magnetic field column using saline as both washing and final eluent buffer. The specific activity of the RNP was 10−15 μCi/mg of RNP.

In vitro cell binding assay of RINP

Purified RINP of each lot was evaluated by in vitro immunoreactivity as % of RINP bound to HBT 3477 cells. Relative immunoreactivity was established by comparing with reference ^{111}In-ChL6 alone used in these studies (21). The ^{111}In-DOTA-ChL6, RINP and viable cells (2×10^7 cells/ml) were diluted to the desired concentrations in phosphate buffered saline (pH 7) to find the maximal binding percentage corresponding to the reported method(22). ^{111}In-DOTA-ChL6 (10 ng) and RINP of each (50 μl, 0.04mg/mL), were added to triplicate tubes. One million cells (50 μl) were added to the triplicates, vortexed, and incubated for 1 h at room temperature. The cells were pelleted by centrifugation at 300 × *g* for 10 min, and the supernatant and cells were counted. The percentage bound was calculated as follows: [cell bound cpm/(cell cpm + supernatant cpm)] × 100.

RINP size measurement

RINP size was measured by dynamic light scattering (photon correlation spectroscopy) using a Zetasizer 3000 (Malvern Instruments Ltd., UK) after suspensions underwent 0.45-μm filtration. This instrument uses a 5-mW He Ne laser (633 nm) and measures particle

sizes from 2 to 3000 nm. Fluctuations in the intensity of scattered light (at 90° to the incident) are analyzed through the use of autocorrelation functions.

Animal Studies

Female (7−9 week old), athymic Balb/c nu/nu mice (Harlan Sprague Dawley, Inc., Frederick, MD) were maintained according to University of California animal care guidelines on a normal diet *ad libitum* and under pathogen-free conditions. HBT 3477 cells were harvested in log phase; 3.0×10^6 cells were injected subcutaneously on both sides of the abdomen of mice for the PK study. Five groups of mice with 9 animals per group and two HBT3477 tumors per mouse were used for the PK study and 3 mice with bilateral HBT3477 were used for WBAR study. RNP negative control (group 1), non immunoreactive RINP (group 2) was studied at 24h and 48h and 20nm, 30nm, and 100nm RINPs experimental groups (groups 3 − 5) were studied at 4, 24, and 48h time points. All mice studies were initiated 2 to 4 weeks after implantation when the tumor volume was 100 − 350 mm^3. PK and WBAR studies were performed using RINP doses of 20−25 μCi per mg of RINP, injected iv into a lateral tail vein with an additional 50 μg ChL6 (cold) in 200 μl saline.

Whole Body Autoradiography (WBAR)

WBAR was conducted, as previously described (23;24). Twenty four hours after tail vein injection of 50μg/50μCi/200μL/5mg of RINP mice were anesthetized using an intravenous injection of 50 mg/ml of 100 μl aqueous solutions of sodium pentobarbital, then flash frozen in a hexane, dry ice bath. The frozen mice were embedded in 4% carboxymethylcellulose and sagittal sections were generated with a Leica Polycut (town, country) at −20° C. Sections of 50 μm thicknesses were obtained to show tumors, spleen, kidney, liver and the midline of the vertebral column. Radiographs of the sections were prepared by exposing the sections to x-ray film (Kodak BioMax MS, Rochester, N.Y.).

Pharmacokinetic Study

RINP doses were injected iv in 200−250 μl saline. In the pharmacokinetic studies, whole body activity was measured in a dose calibrator (CRC-12, Capintech, Inc., Pittsburgh, PA) immediately, and again 1, 4, 24 and 48 hours and values were expressed as %ID. Blood activity, expressed as %ID/ml, was determined by counting 2 μl blood samples, collected at 5 min, 1, 4, 24 and 48 hours after injection in a gamma well counter (Pharmacia LKB, Piscataway, NJ) calibrated using ^{111}In standards in the appropriate sample configuration and volumes. The mice were sacrificed and organs and tissue samples collected. Activity, expressed as %ID/g, was measured in a gamma well counter in a manner similar to that used for blood activity (25). Specific activity and dose used for animal study was 20−25μCi/ 5−10μg of MAb/2.2 mg RINP or non immunoreactive RINP.

RESULTS

Preparation, Characterization and Quality Assurance of RIC, RNP, and various RINP

Figure 1 shows a simple schematic diagram of a representative NF-type RINP. Table 1 indicates the specification of various sizes of RINP. The purified RIC molecule of ^{111}In-DOTA-Bz-ChL6 was evaluated by CAE, HPLC and PAGE prior to conjugation to NP. The specific activity of the RIC was 0.5 μCi/μg with greater than 95% monomeric by HPLC, CAE and PAGE (Figure 2A, lane # 0 and Figure 2B, lane #1 and 3). The absolute binding of RIC in the live cell assay was > 70% and equal to100% compare to ^{125}I-ChL6 as reference standard. The RIC used for non immunoreactive RINP (20nm) was 4 % compared to ^{125}I-ChL6 as reference standard. Using carbodiimide chemistry, RINP products were prepared

by conjugation of ^{111}In-DOTA-Bz-ChL6 to COOH functionalized NP of 20-nm and 30 and 100-nm particles; and the amount of ^{111}In-ChL6 linked to NPs were 5, 4 and 3 (μg/mg) respectively. In the case of non immunoreactive RINP the ^{111}In-ChL6 (non immunoreactivity) was linked to 20 nm NP with 6 μg/mg of NP. Similarly particles of without targeting molecules as nontargeting 20nm NP (RNP) was prepared for the negative control (10μCi/mg) using ^{111}In-DOTA-Bz-NH_2 and 20 nm NP.

All of the RINP's were greater than 90% monomeric by PAGE (Figure 2A-B) and CAE (Figure 3). Each purified RINP was a dark brown, homogeneous suspension and remained at the origin of PAGE. The RINPs (20, 30 and 100 nm) shown in figure 2A, by Coomassie lanes 1− 3 and radioactivity in lanes 4 −6, did not migrate due to the high molecular weight. However, no unbound ChL6 or ^{111}In-DOTA-ChL6 was observed, corresponding to the control protein in Figure 2A lane #0, and Figure 2B lane 1 or control radiolabeled ChL6 in lane 3. Figure 3 shows the evaluation of the RINP mobility by CAE at 11 min (lanes # 1, 3 and 5) and 45 min (lanes # 2, 4 and 6). These preparations are >90% monomeric with no aggregation or unbound free ChL6. The specific activity of the final purified RINP was 6−8 μCi /3−5 μg of ^{111}In-ChL6/mg of NP. The concentration of ^{111}In-ChL6 conjugated to NP was estimated by decay corrected specific activity of the RINP and the ^{111}In-ChL6 conjugated to each NP was as 6−10 molecules per bead.

Using photon correlation spectroscopy, the size of the RINP were (Figure. 4) distributed to narrow diameter ranges of 20−30, 30−40, and 70−100 nm. RINP sizes did not change compared to NP size prior to conjugation with ^{111}In-MAb (12). Thus RIC conjugation on NP did not influence or alter the initial particle diameters.

In vitro Cell Binding Assay

The radioimmunoassay (RIA) of RIC and RINP was tested using HBT 3477 human breast cancer cells. Relative immunoreactivity of the RINP showed 57−79 % compared to control RIC tested on HBT 3477 (Table 1).

WBAR and PK in mice

The WBAR obtained from a mouse sacrificed 24 h after injection of the 100nm RINP, showed that the particles were able to target tumor in vivo (Figure 5). Blood and body clearances of the RINP (Figure 6-7) and mean RINP concentrations (%ID/g) in lung, kidney and lymph node (Figure 8) were similar to ^{111}In-ChL6-NP as previously reported (7). In vivo tumor targeting of RINPs were compared with RNP (without the targeting MAb molecules) and non immunoreactive RINP (20nm). Figure 8 shows mean concentrations of RINP of each preparation in tumor in the PK study were between 4 − 9 % ID/g over 2 days. RNP 20nm NP with no targeting molecules and non immunoreactive RINP (20nm) was used as a negative control and demonstrated (Figure 8) tumor accumulation of less than 0.5 % ID/g. The differences of tumor uptake observed between the targeted and nontargeted NPs were substantial. The 20-nm RINP tumor uptake showed consistent with previous observations (5; 7). Both 30-nm and 100-nm BNF particles demonstrated a lower tumor uptake than SPIO's, with little difference between the two.

DISCUSSION

Focused hyperthermia (FH) can be achieved at selective cancer tissues by ligand directed magnetic nanoparticles using AMF to activate NP to deliver heat (26). This treatment modality is more advantageous than other thermo therapies, because heat is induced locally by external AMF application through activation of cancer targeted nanoparticles which are preferentially retained in the microenvironment of the tumor tissues at higher concentrations

than in the immediately surrounding normal tissues (27; 28). In this approach the AMF is field preferentially directed to the regions containing cancer (11), and the field amplitude can be adjusted to provide NP heat lethal only at the cancer tissues while minimizing the heat deposited elsewhere thus sparing the surrounding normal tissues. To enhance the FH, high SAR NF-type particles were developed (12). Two sizes of these NF-type particles were evaluated in this study to characterize their in vivo performance in comparison with a previously used 20-nm SPIO particle. Future selection of a preferred RINP will be based on two criteria: 1) concentration of the particles targeted at the tumor; and 2) particle SAR heat after AMF activation.

Three types of RINP were created using the 20-nm (SPIO) and 30-and 100-nm (NF) particles linked to ^{111}In-ChL6 to target breast cancer in mice. In our previous study we have demonstrated that RINP based on 20-nm SPIO particles were successfully utilized for thermal therapy in a mouse model (7). However, the SPIO particle SAR value was not sufficient to induce enough heat to eradicate the cancer completely with modest amplitudes of AMF at a frequency of 150 kHz.

In this study we have compared 30 and 100-nm RINP from NF particles with previously tested 20-nm SPIO RINP. All of these preparations had a high purity and excellent immunoreactivity and were similar to the preparation used in the earlier therapy studies. The in vivo PK and WBAR study showed 100 nm RINP accumulations in tumor was 50% of that of the 20nm SPIO RINP. However, the SAR value of 100-nm particles has been measured to be up to 6 times higher (Table 2) than the 20-nm SPIO particles. Therefore the calculated net heat induction for any specific AMF in cancer tissue by 100-nm RINP is expected to be three times higher than that produced by 20-nm RINP (SPIO).

Important characteristics of magnetic NP for FH applications are narrow particle size distribution and high SAR values providing substantial heat at lower AMF (29). In general, RINP accumulation at the tumor tissues depends on the RINP affinity, the presence of abundant cancer cell targets for the molecules linked to NP, circulation half time, and tumor vessel permeability. The NP of SPIO and NF preparations were different in surface morphology, physical characteristics (density), surface charge, PEG concentration and functional modification which may affect the PK. The cellular and tissue uptake was effected by several characteristics of the nanoparticles e.g., particle size, coatings, and charge as demonstrated by Wu et al.,(30). In another study surface properties had a larger impact on cellular uptake of SPIO particles rather than particle size (31). In our study ^{111}In-DOTA conjugated RNP (negative control) showed less than 5% uptake in liver and spleen compared to RINPs which showed above 10% as shown in Figure 8. This may be due to increased anionic charge of the RNP. However, this was not the focus of this study. NP design and chemical conjugation were optimized in such a way that RINP preparations were fully functional to target the antigen both in vitro and in vivo. The particles were also coated with PEG molecules to increase plasma half-time and decrease uptake in normal tissues. The present study clearly confirms that the NF based 100 nm RINP are able to penetrate the tumor vessels sufficiently well for moderate tumor accumulation (see Figure 5 and 8). In conclusion, we have created RINP of varying sizes using SPIO and NF NP to target breast cancer for focused hyperthermia. Analytical methods have been developed to characterize the RINP. Radiotracer was utilized on NP to establish RINP targeting in the tumor, to predict thermal dose in the tumor and quantify RINP tissue biodistributions. Although 100nm NF RINP targeted tumor less than 20nm SPIO RINP, because their heating capacity was 6 times higher, 100nm BNF RINP should provide three times greater heat dose in tumor with AMF activation. A complete characterization of the physical and magnetic properties of these particles, and how these are affected by the chemical modifications of the surface coatings is underway.

Acknowledgments

This work was supported by US Army Medical and Materiel Command under Contract Number W81XWH-04-C-0142 and National Cancer Institute NCI grant PO1-CA47829.

LITERATURE CITED

1. Ito A, Honda H, Kobayashi T. Cancer immunotherapy based on intracellular hyperthermia using magnetite nanoparticles: a novel concept of “heat-controlled necrosis” with heat shock protein expression. Cancer Immunol Immunother. 2006; 55:320–328. [PubMed: 16133113]
2. Gref R, Couvreur P, Barratt G, Mysiakine E. Surface-engineered nanoparticles for multiple ligand coupling. Biomaterials. 2003; 24:4529–4537. [PubMed: 12922162]
3. Rudershaun R, Gruttner C, Frank M, Teller J, Westphal F. Multifunctional Superparamagnectic Nanoparticles for Life Science Applications. European Cells Materials. 2002; 3:81–83.
4. Jordan, A.; Hauff-maeir; Wust, P.; Johannsen, M. Nanoparticles for Thermotherapy. In: Kumar, CSSR., editor. Nanaomaterials for cancer Therapy. WILEY-VCH; Weinheim: 2006. p. 242-258.Chapter 8
5. DeNardo SJ, DeNardo GL, Miers LA, Natarajan A, Foreman AR, Gruettner C, Adamson GN, Ivkov R. Development of tumor targeting bioprobes (^{111}In-chimeric L6 monoclonal antibody nanoparticles) for alternating magnetic field cancer therapy. Clin. Cancer Res. 2005; 11:7087s–7092s. [PubMed: 16203807]
6. Ito A, Tanaka K, Honda H, Abe S, Yamaguchi H, Kobayashi T. Complete regression of mouse mammary carcinoma with a size greater than 15 mm by frequent repeated hyperthermia using magnetite nanoparticles. J Biosci. Bioeng. 2003; 96:364–369. [PubMed: 16233538]
7. DeNardo SJ, DeNardo GL, Natarajan A, Miers LA, Foreman AR, Gruettner C, Adamson GN, Ivkov R. Thermal dosimetry predictive of efficacy of 111In-ChL6 nanoparticle AMF-Induced thermoablative therapy for human breast cancer in mice. J Nucl Med. 2007; 48:437–444. [PubMed: 17332622]
8. Dewhirst, MW.; Jones, E.; Samulski, T.; Vujaskovic, Z.; Li, C.; Prosnitz, L. Hyperthermia. In: Kufe, D.; Pollock, R.; Weichselbaum, R.; Bast, R.; Gansler, T.; Holland, J.; Frei, E., editors. Cancer Medicine. 6th ed.. BC Decker, Inc.; Hamilton, Ontario: 2003. p. 623-636.
9. Van der ZJ. Heating the patient: a promising approach?. Ann Oncol. 2002; 13:1173–1184. [PubMed: 12181239]
10. Dewhirst MW, Viglianti BL, Lora-Michiels M, Hanson MW, Hoopes PJ. Basic principles of thermal dosimetry and thermal thresholds for tissue damage from hyperthermia. Int J Hyperthermia. 2003; 19:267–294. [PubMed: 12745972]
11. Ivkov R, DeNardo SJ, Daum W, Foreman A, Goldstein R, DeNardo GL. Application of high amplitude alternating magnetic fields for heat induction of nanoparticles localized in cancer. Clin. Cancer Res. 2005; 11:7093s–7103s. [PubMed: 16203808]
12. Gruttner C, Muller K, Teller J, Westphal F, Foreman A, Ivkov R. Synthesis and antibody conjugation of magnetic nanoparticles with improved specific power absorption rates for alternating magnetic field cancer therapy. Journal of Magnetism and Magnetic Materials. 2007; 311:181–186.
13. Grüttner, C.; Teller, J.; Schütt, W.; Westphal, F.; Schümichen, C.; Paulke, BR. Scientific and Clinical Applications of Magnetic Carriers. Häfeli, UO.; Schütt, W.; Teller, J.; Zborowski, M., editors. Plenum Press; New York: 1997. p. 53
14. Rudershausen S, Gruttner C, Frank M, Teller J, Westphal F. Multifunctional Superparamagnetic Nanoparticles for life science applications. European Cells and Materials. 2002; 3:81–83.
15. Schütt W, Grüttner C, Teller J, Westphal F, Häfeli UO, Paulke BR, Goetz P, Rutz W, Putzar H, Dunkelmann S, Finck W, Schümichen C. The concept of magneto-radionuclide-therapy. Jpn. J. Electroph. 1997; 47:173−179.
16. Liu AY, Robinson RR, Hellstrom KE, Murray EDJ, Chang CP, Hellstrom I. Chimeric mouse-human IgG1 antibody that can mediate lysis of cancer cells. Proc. Natl. Acad. Sci. U. S. A. 1987; 84:3439–3443. [PubMed: 3106970]

17. Hellstrom I, Horn D, Linsley P, Brown JP, Brankovan V, Hellstrom KE. Monoclonal antibodies raised against human lung carcinomas. Cancer Res. 1986; 46:3917–3923. [PubMed: 3731064]

18. Josephson L, Tung CH, Moore A, Weissleder R. High-efficiency intracellular magnetic labeling with novel superparamagnetic-Tat peptide conjugates. Bioconjug. Chem. 1999; 10:186–191. [PubMed: 10077466]

19. McCall MJ, Diril H, Meares CF. Simplified method for conjugating macrocyclic bifunctional chelating agents to antibodies via 2-iminothiolane. Bioconjug. Chem. 1990; 1:222–226. [PubMed: 2096914]

20. Natarajan A, Xiong CY, Gruettner C, DeNardo GL, DeNardo SJ. Development of multivalent radioimmunonanoparticles for cancer imaging and therapy. Cancer Biother. Radiopharm. 2008; 23:82–91. [PubMed: 18298332]

21. Kukis DL, DeNardo GL, DeNardo SJ, Mirick GR, Miers LA, Greiner DP, Meares CF. Effect of the extent of chelate substitution on the immunoreactivity and biodistribution of 2IT-BAT-Lym-1 immunoconjugates. Cancer Res. 1995; 55:878–884. [PubMed: 7850803]

22. Winthrop MD, DeNardo SJ, Albrecht H, Mirick GR, Kroger LA, Lamborn KR, Venclovas C, Colvin ME, Burke PA, DeNardo GL. Selection and characterization of Anti-MUC-1 scFvs intended for targeted therapy. Clin. Cancer Res. 2003; 9:3845s–3853s. [PubMed: 14506182]

23. Fand, I.; McNally, WP. The technique of whole-body autoradiography. In: Johnson, JE., editor. Current trends in morphological techniques. 1 ed.. CRC Press; Boca Raton, FL: 1981. p. 1-28.

24. DeNardo GL, Kroger LA, DeNardo SJ, Miers LA, Salako Q, Kukis DL, Fand I, Shen S, Renn O, Meares CF. Comparative toxicity studies of yttrium-90 MX-DTPA and 2-IT-BAD conjugated monoclonal antibody (BrE-3). Cancer. 1994; 73:1012–1022. [PubMed: 8306243]

25. DeNardo SJ, Burke PA, Leigh BR, O'Donnell RT, Miers LA, Kroger LA, Goodman SL, Matzku S, Jonczyk A, Lamborn KR, DeNardo GL. Neovascular targeting with cyclic RGD peptide (cRGDf-ACHA) to enhance delivery of radioimmunotherapy. Cancer Biother. Radiopharm. 2000; 15:71–79. [PubMed: 10740655]

26. Hilger I, Hiergeist R, Hergt R, Winnefeld K, Schubert H, Kaiser WA. Thermal ablation of tumors using magnetic nanoparticles: an in vivo feasibility study. Invest Radiol. 2002; 37:580–586. [PubMed: 12352168]

27. Wust P, Gneveckow U, Johannsen M, Bohmer D, Henkel T, Kahmann F, Sehouli J, Felix R, Ricke J, Jordan A. Magnetic nanoparticles for interstitial thermotherapy--feasibility, tolerance and achieved temperatures. Int J Hyperthermia. 2006; 22:673–685. [PubMed: 17390997]

28. Jordan A, Scholz R, Maier-Hauff K, van Landeghem FK, Waldoefner N, Teichgraeber U, Pinkernelle J, Bruhn H, Neumann F, Thiesen B, von DA, Felix R. The effect of thermotherapy using magnetic nanoparticles on rat malignant glioma. J Neurooncol. 2006; 78:7–14. [PubMed: 16314937]

29. Kim DH, Lee SH, Im KH, Kim KN, Kim KM, Shim IB, Lee MH, Lee YK. Surface-modified magnetite nanoparticles for hyperthermia: Preparation, characterization, and cytotoxicity studies. Current Applied Physics. 2006; 6:e242–e246.

30. Wu YJ, Muldoon LL, Varallyay C, Markwardt S, Jones RE, Neuwelt EA. In vivo leukocyte labeling with intravenous ferumoxides/protamine sulfate complex and in vitro characterization for cellular magnetic resonance imaging. Am J Physiol Cell Physiol. 2007; 293:C1698–C1708. [PubMed: 17898131]

31. Metz S, Bonaterra G, Rudelius M, Settles M, Rummeny EJ, Daldrup-Link HE. Capacity of human monocytes to phagocytose approved iron oxide MR contrast agents in vitro. Eur Radiol. 2004; 14:1851–1858. [PubMed: 15249981]

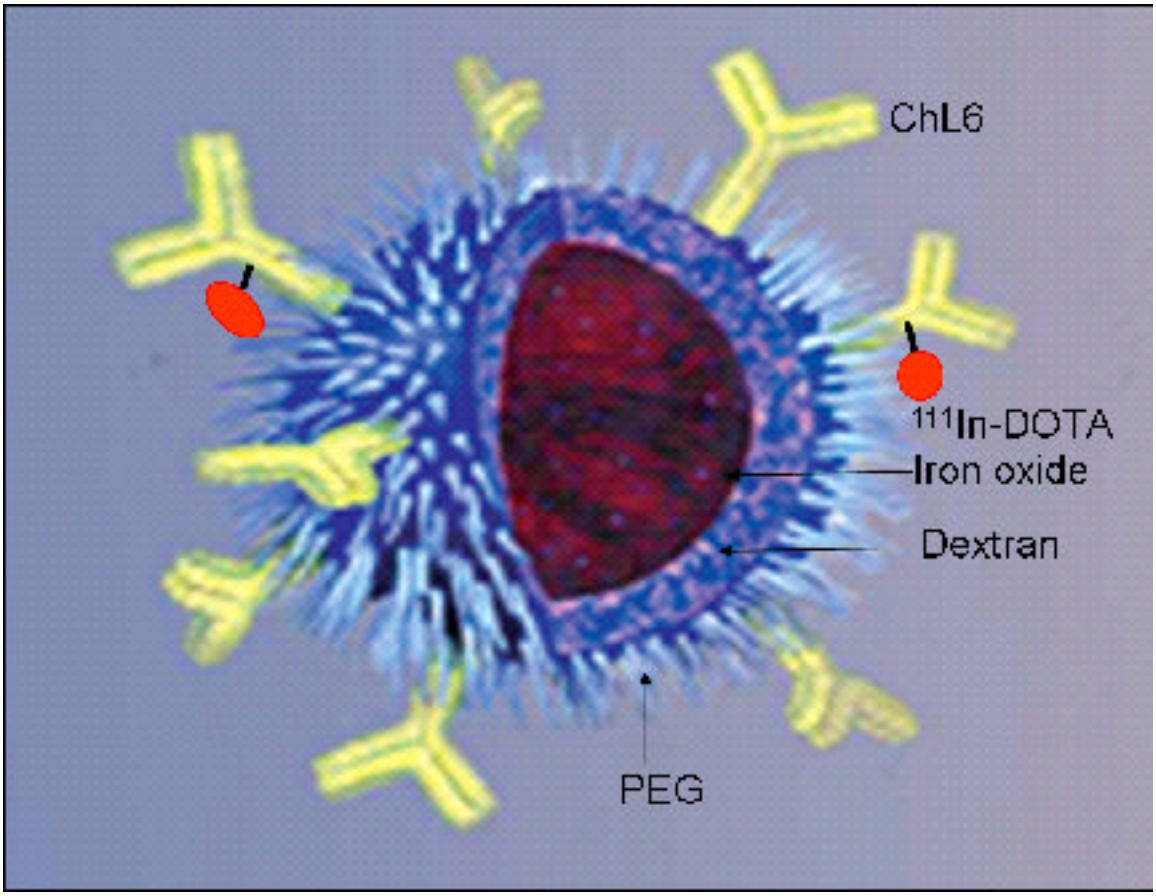

Figure 1.
Simple diagram of a BNF-type particle coated with PEG to link ^{111}In-ChL6 to construct RINP. The particle core (reddish brown sphere in center) is iron oxide.

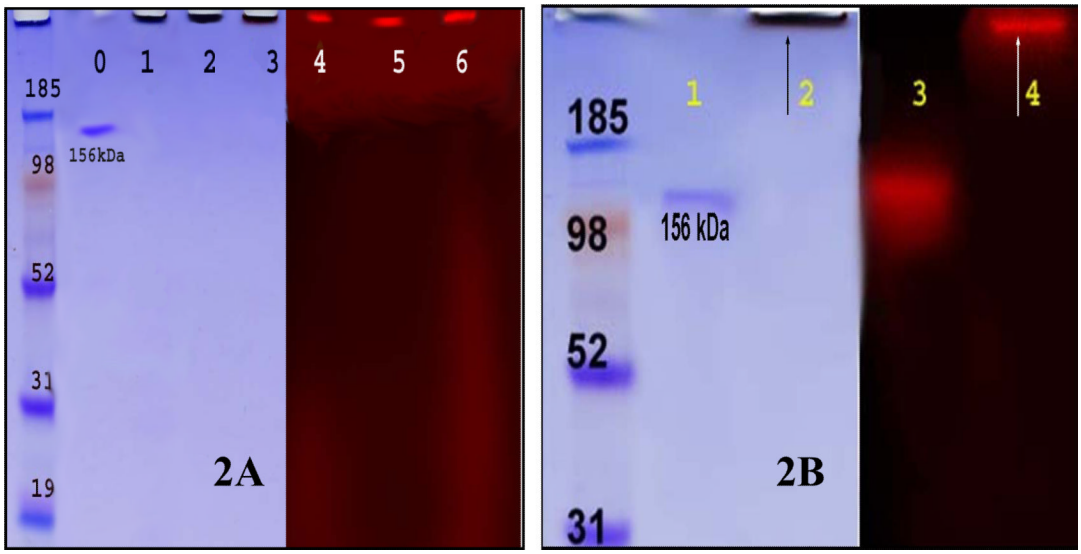

Figure 2.

RINP on 4−12% SDS - PAGE spectrum; Left: CB stained for protein detection and right: same PAGE scanned on Fuji phosphor Imager for radioactivity detection. **Figure 2A**: RINP (20, 30, and 100 nm) on 4−12% SDS - PAGE spectrum; Lane # 0: ^{111}In-DOTA-Bz-ChL6; lane #1−3: RINP (20, 30 and 100 nm) - brown band at origin, no unconjugated ^{111}In-ChL6 observed; lane # 4− 6: radioactivity bands are at origin corresponds to RINP (20, 30, and 100nm). **Figure 2B**: Lane #1: ^{111}In-DOTA-Bz-ChL6; lane #2: RINP (100 nm) - brown band at origin; lane #3: ^{111}In-DOTA-Bz-ChL6 and lane #4: radioactivity band at origin corresponds to RINP.

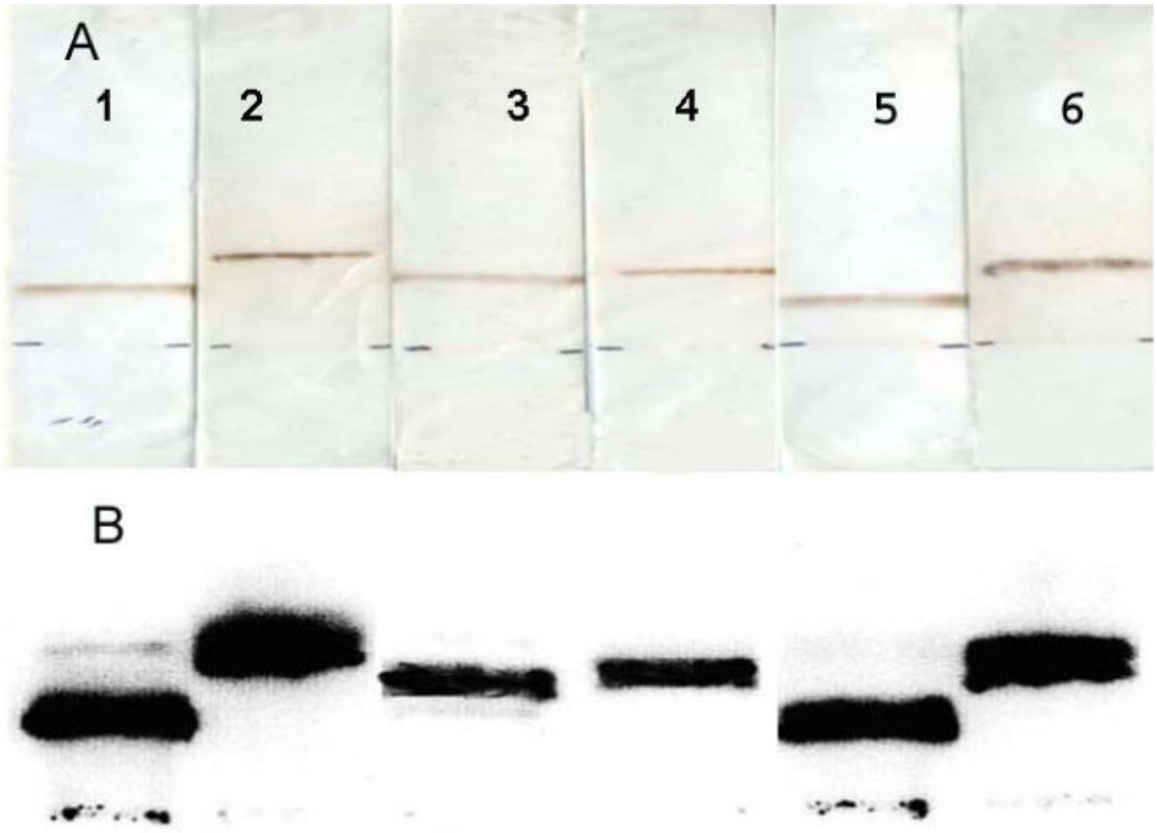

Figure 3.

CAE characterization of RINPs.111-In-ChL6 modified NPs of 20nm (lanes 1&2), 30nm (lanes 3&4), and 100nm (lanes 5&6) were tested on CAE strips, using pH 8.5 buffer, 300volts, at 11 min (lanes 1, 3 and 5) and 45 min (lanes 2, 4 and 6) time points. A) RINPs tested on CAE strips were scanned by laser (scanner brown bands correspond to iron oxide of NPs visible at different distance from the origin (2cm above from bottom of the strip). B) The same CAE strips were scanned on Fuji Imager to analyze the migration pattern of RINPs by size and charge effect traced by radioactivity. The migration distances of each lot of NPs have identical distance by radioactivity and band stain. RINPs preparations were greater than 95% pure. The purity of the RINP on CAE 11min and 45 min showed greater than 90% monomeric product. RINP preparation does not contain aggregated particles or free ^{111}In-ChL6 molecules

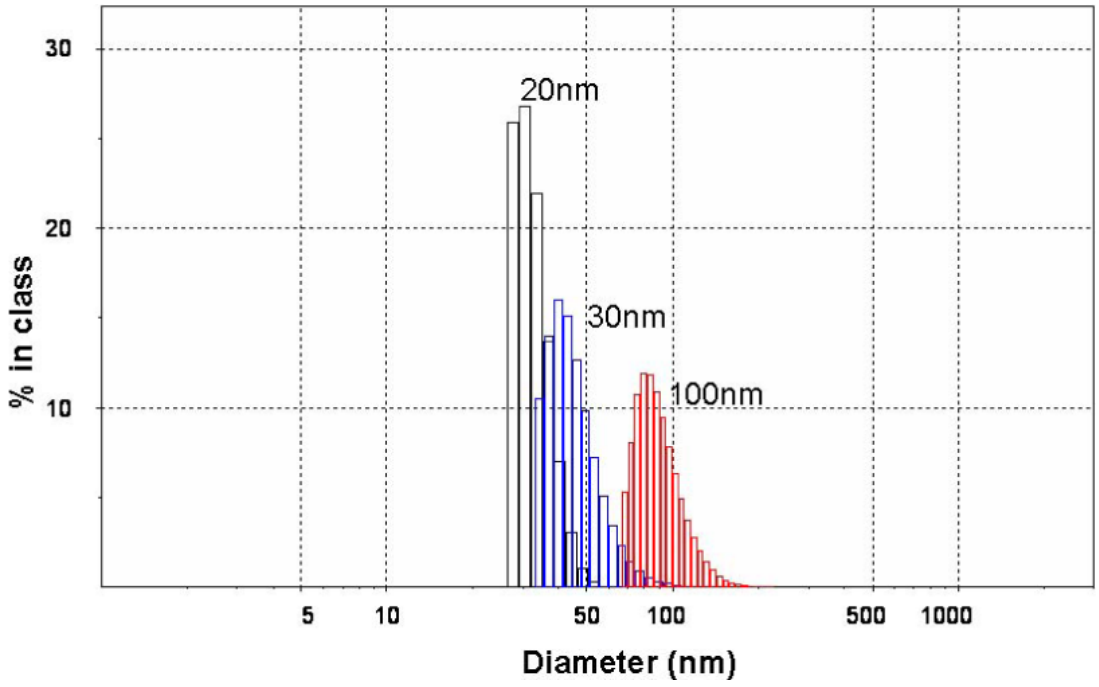

Figure 4.
RINP Size distributions were measured by photon correlation spectroscopy (Zetasizer 3000, Malvern Instruments, Ltd.).

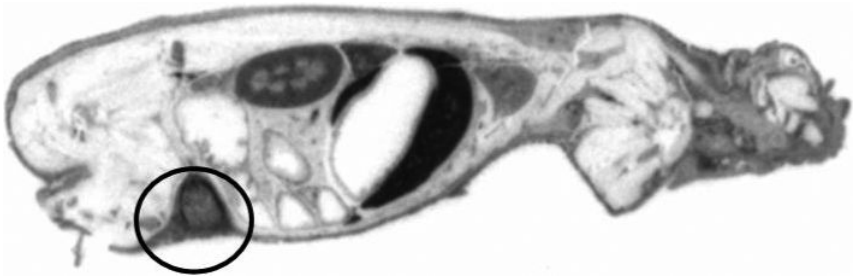

Figure 5.

Sagittal section of the WBAR image was obtained euthanized mice after 24h tail vain injection of ^{111}In-ChL6-NP (100nm- BNF). The HBT3477 tumor (human breast cancer) bearing nude mice received 50μCi/5mg of RINP dose. Accumulations of RINPs are mostly in kidney, liver, and tumor (circle).

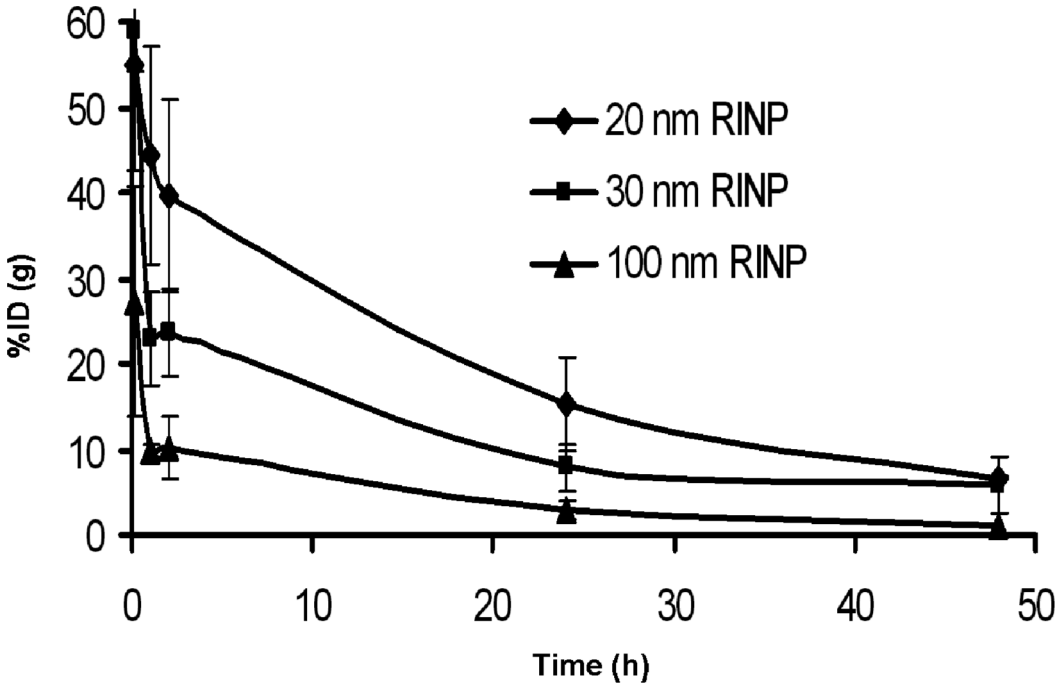

Figure 6.
Pharmacokinetic study of RINPs in mice with HBT3477 human breast cancer xenografts (nine animals per group) three groups of total. Three RINPs blood clearances were compared at various time points; 5 minutes, 1, 2, 4, 24 and 48h.

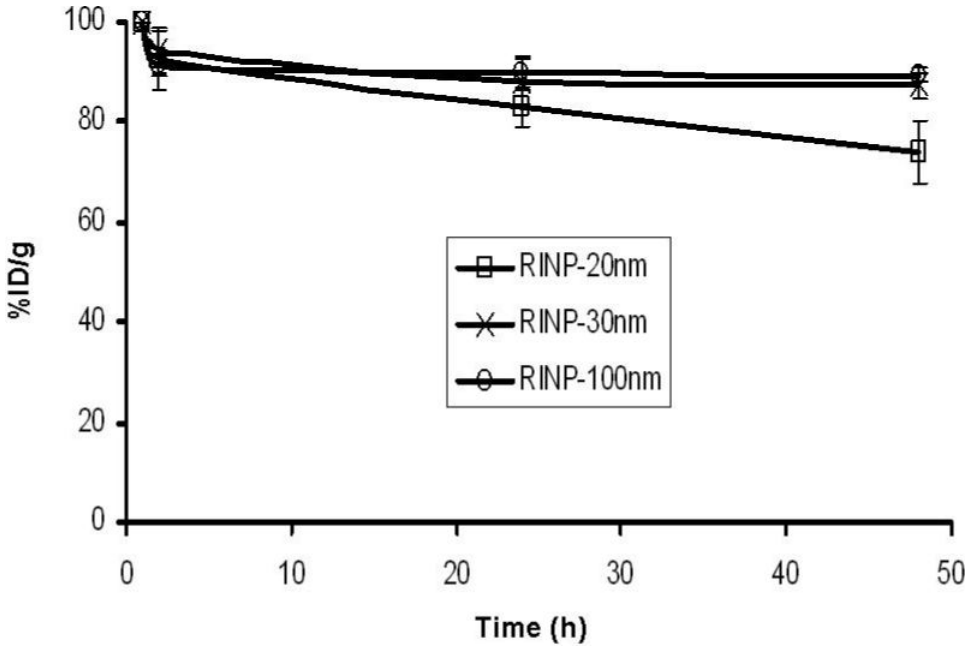

Figure7.

The pharmacokinetic study of three RINPs (20, 30 and 100nm) in mice with HBT3477 human breast cancer xenograft was used. Body clearances were compared at various time points of 2, 4, 24 and 48 h. (nine animals per group total five groups were used; non immunoreactive RINP (20nm) and RNP (20nm) negative control groups did not presented in this data).

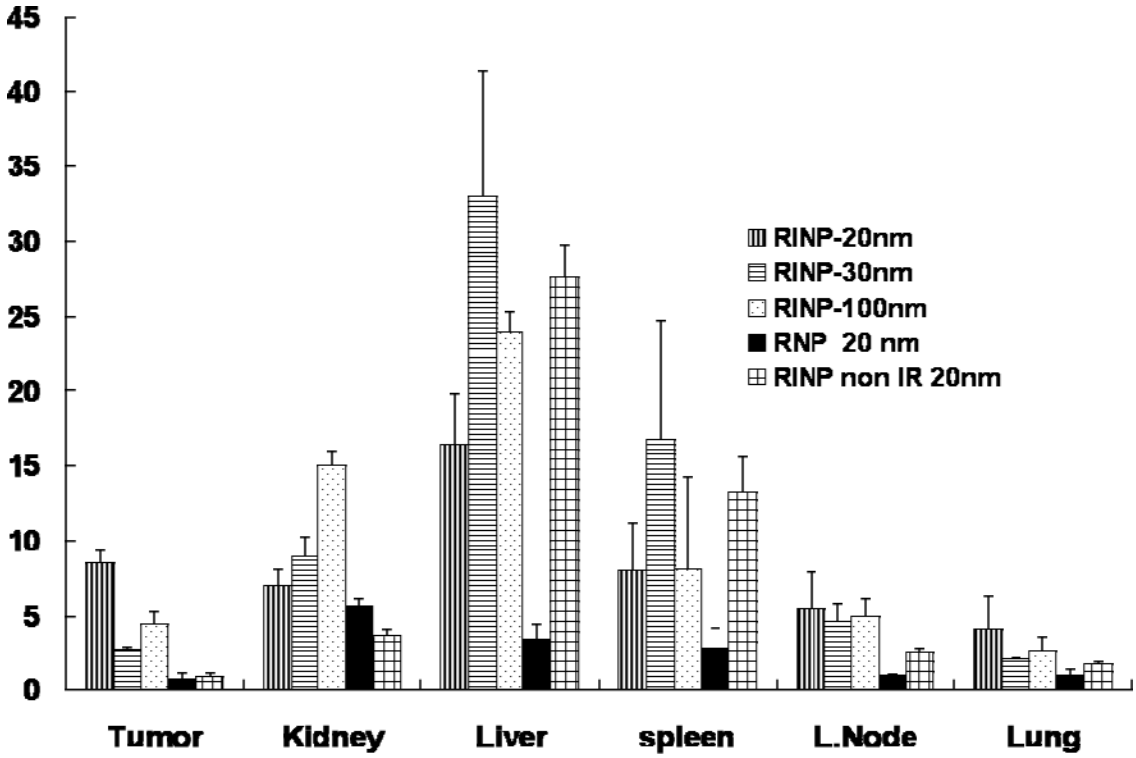

Figure 8.

Pharmacokinetic biodistribution of the RINPs (20nm, 30nm, and 100nm size), negative controls of RNP (20nm) NP without targeting molecules, and RINP (20nm) non immunoreactive were measured as %ID/g in various organs after 48 h injection. The difference between targeted (RINP) and nontargeted particles (RNP) and non immunoreactive RINP (Reference # 5) should be noted. The mean ± SD (error bars) were calculated based on three animals (n =3) in each study group. IR = immunoreactive.

Table 1

Specification of RINP

(NP size nm	Initial NP (mg)	[Fe]/[NP] mg/mg	RINP Yield (mg)	[RIC] μg/mg of NP	SA μCi/mg of RINP	QA		
						CAE 45′ %	PAGE %	RIR %
20	50	0.46	26	5	8	95	90	79
30	50	0.63	26	4	7	75	85	57
100	50	0.6	35	3	6	90	90	60

SA: Specific Activity; RIR: Relative Immunoreactivity.

Table 2

SAR values for BNF- and SPIO-type particles as reported in Reference #12

Nanoparticle type (diameter)	SAR (W/g iron)			
	29 kA/m	58 kA/m	86 kA/m	104 kA/m
20 nm SPIO	27	66	76	105
30 nm BNF	90	253	380	438
100 nm BNF	140	437	528	642

SAR values measured for different mean diameters NP as a function of the amplitude of the AMF